Physica Medica 136 (2025) 105045

Contents lists available at ScienceDirect

Physica Medica

journal homepage: www.elsevier.com/locate/ejmp

Development of an anthropomorphic phantom of the lower extremities for feasibility studies and verification of total-body irradiation

M. Wegner [a,b,*], N.Alizadeh Azbari [b], D. Krause [a], E. Gargioni [b]

[a] Institute of Product Development and Mechanical Engineering Design, Hamburg University of Technology, Hamburg, Germany
[b] Department of Radiotherapy and Radiation Oncology, University Medical Center Hamburg-Eppendorf, Hamburg, Germany

ARTICLE INFO

Keywords:
Phantom
Additive manufacturing
3D printing
Dosimetry
Total-body irradiation
Leg phantom

ABSTRACT

Background: Total-body irradiation (TBI) is a specialised radiotherapy treatment used alongside chemotherapy to prepare leukaemia patients for stem cell transplants. For commissioning and validation of conformal irradiation techniques, anatomically detailed phantoms of the whole body play an important role. This study aimed to create a cost-effective modular phantom of the lower extremities that can be combined with a commercial torso phantom, thus enabling the optimisation of TBI treatment planning and dose delivery.

Methods: We designed a modular leg phantom consisting of five key components: foot, calf, knee, thigh, and hip. Variants of knee and hip allow for both straight and angled leg positions. Inserts for dosimeters are integrated into the knee and hip joints, as well as within femur and fibula. To assess the phantom functionality in TBI, we analysed a currently used static-field technique and studied the feasibility of an intensity-modulated sweeping-beam technique.

Results: We employed 3D printing to create hollow structures of bones, pelvis, and legs, which we filled with surrogate materials representing soft tissue and bone marrow. We simulated cortical bone with a gypsum coating. The CT numbers of soft tissue and bone surrogates align accurately with literature data. The material properties remained stable even one-year post-manufacturing, ensuring long-term use of the phantom. First dose verification measurements for the static-field technique show an agreement with the prescribed dose within less than ±10 %.

Conclusion: The cost-effective modular phantom can be combined with a commercial torso phantom, allowing for the optimization and verification of various CT-based TBI techniques.

1. Introduction

Total-body irradiation (TBI) is a specialized form of treatment, which, in combination with chemotherapy, is often used to prepare leukaemia patients for bone marrow stem cell transplants [1]. By irradiating the entire body, the immune system is suppressed to prevent rejection of the transplanted stem cells [2]. If using high TBI doses, i.e., of the order of 12 Gy, the treatment is myeloablative and has the purpose of destroying tumour cells, particularly in sites that cannot be reached by chemotherapy (such as the brain). Quality assurance is crucial in TBI, as successful treatment requires delivering a sufficiently homogeneous dose to the whole body, with relative deviations from the prescribed dose within ±10 % [3]. However, it is equally important to reduce dose to certain radio-sensitive organs in order to minimize side effects and long-term damage [3–5].

Well-established TBI techniques employ rectangular opposing fields in different combinations. For high-dose myeloablative regimens, these techniques involve the use of metal absorbers to reduce lung dose [6]. Also, thanks to recent technological improvements, modern irradiation techniques are evolving towards intensity modulation, with irradiations taking place either on the treatment couch or at extended source-to-surface distance (SSD) [7–12]. Independent on the implemented technique, it is of paramount importance to accurately plan and delivery TBI. Conformal techniques need CT images of the whole body, a fast method for contouring, the development of planning protocols, accurate dosimetry, and image verification [13]. Existing approaches for implementing sophisticated TBI techniques are heterogeneous, therefore, in the future, dosimetry audits for TBI will become necessary, as recently discussed by Misson-Yates *et al.* [12]. In fact, dosimetry audits and commissioning of new techniques play an important role in every field

* Corresponding author.
E-mail address: marie.wegner@tuhh.de (M. Wegner).

https://doi.org/10.1016/j.ejmp.2025.105045
Received 14 February 2025; Received in revised form 13 June 2025; Accepted 4 July 2025

of radiotherapy. Audits, in particular, ensure a high level of dosimetric accuracy and are thus necessary to participate in clinical trials [14].

Physical anthropomorphic phantoms play a crucial role in quality assurance for radiotherapy by enabling accurate image-based dose calculations and plan optimization. Moreover, these phantoms provide a reliable physical anatomical model for ensuring precise dose measurements during irradiation. However, commercially available phantoms of the whole body, as well as add-ons for extremities, are very expensive and are typically designed for a specific purpose. Also, they are not suitable for dosimetry in their standard configuration [15–17]. Therefore, in most cases, TBI dose verification is carried out with simple geometrical phantoms (cylinders, slabs) or anthropomorphic phantoms of the sole torso [12].

The aim of this work was therefore to develop and manufacture a cost-effective tissue-equivalent leg phantom, which can be combined with a commercial upper-body phantom to form a whole-body phantom for quality assurance and optimisation of TBI and further whole-body techniques, such as total-marrow or total-nodal irradiations. Different leg positions will make it possible to optimize treatment planning, compare different techniques, and verify dose at standard and extended SSD.

2. Materials and methods

For the development of the leg phantom, we used the workflow for 3D printed phantoms presented in Wegner and Krause [18]. This methodological approach structures the development, similar to the standard VDI 2221 of the German Association of Engineers [19], into four phases: (i) planning, (ii) concept, (iii) design, and (iv) validation. While the first three phases are described in this section, the validation of the phantom will be part of the results section. Since the phantom is intended for use in TBI studies, we will describe in the following some application examples.

2.1. Phantom planning

A very important step during phantom planning is the collection of requirements. With the help of a survey tool that we developed in previous work [20], we collected requirements for a quality assurance phantom to be used in radiotherapy and in computed tomography (CT), as shown in Table 1. In particular, the phantom developed in this work should extend the commercial Alderson Radiation Therapy (ART) phantom (Radiology Support Devices Inc., CA, USA), which is an upper-body phantom. Furthermore, due to the variety of available TBI techniques, it should be possible to arrange the legs in a straight position, with the help of patient knee and foot pillows, as well as in a bent position, where no pillows are needed and the feet are flat on the patient table. The set-up should be reproducible for CT imaging and for irradiation at a linear accelerator. Dosimetry should be possible in different locations with different detectors as well as with dosimetry films. For an accurate dose calculation, the phantom materials should mimic soft tissue, bone marrow, and cortical bone, respectively.

2.2. Phantom concept

A side view of the derived phantom concept in both positions is displayed in Fig. 1. The concept image is based on a Modular Interface Graph (MIG) [21,22], which is used in product development to illustrate the components of a product family and their class (standard, variant, optional, or individual). The phantom components are: foot, calf, knee, thigh, and hip. Among these components, three are standard, while knee and hip are variants for the two leg positions (flat and bent, respectively). This means that the final phantom will comprise two modules for knee and hip, which are specific for each position. On the one hand, we disregarded a joint solution for knee and hip, since the joint mechanism would have taken too much space. On the other hand, we could implement a joint solution for the foot, so that it can be adjusted between the flat and bent position. Each phantom component will be mirrored after design resulting in a left and right leg, which thus will be symmetrical.

Table 1
Excerpt of the requirements collected for the leg phantom.

Category			Answered Phantom Requirement
Classifying Characteristics	Type		Physical
	Purpose		Quality assurance (Dosimetry)
	Area of application	Medical imaging	CT
		Image-guided therapy	Yes, Radiotherapy
	Anatomy	Topographical anatomy	Lower extremities
		Organs/ tissues	Bone (cortical and bone marrow), soft tissue
Degree of Reality	Geometrical mapping		Object based
	Physiological mapping		Quasi-static
	Image modality mapping		Realistic/ high
	Medical therapy mapping		Realistic/ high
Custom Design Characteristics	Production		In-house
	Dosimetry		Yes, radiochromic film, ionization-chamber, OSL-chips
	Size dimensions		Maximal length 100 cm
	Shelf-life-time (Stability)		Medium shelf-life (a few months to one year)
	Production costs		Material costs under 200€
	Transportability		Transportable; under 10 kg weight
	Reproducibility		Reproducible set-up of the phantom both for imaging and irradiation
	Other		Two leg positions needed, 1. flat on patient pillows (10°) and 2. bent on table (45°)
			Needs to be connected to the ART upper body phantom
			Dosimetry Insert 2 × 2 cm

To identify suitable tissue surrogates, we carried out initial material tests, using cylindrical samples, before selecting the final surrogate mixtures. The key criterion was to achieve corresponding tissue-equivalent CT numbers. During material selection, we decided to use 3D printing for the direct production of the legs. In particular, we found that the 3D printing of the phantom outer shell and the hollow shell of the bone structure would be more effective, with a consequent addition of surrogate mixtures during post-processing.

2.3. Phantom design

To design the connection between the leg phantom and the ART upper body phantom, we created 3D models of bones and body shape. These models are useful to accurately position the bones within the leg phantom and to design its external shape at the connection point. The 3D models were generated from a CT scan of the ART phantom using *3D Slicer* [23] (Fig. 2a,b). A similar process was followed for the patient pillows to ensure proper fitting of the final legs. Freely available D stereolithography (STL) models of femur, tibia, and fibula were sourced from the online database Sketchfab (Sketchfab, Inc., NY, USA). All STL models were arranged and post-processed using *Autodesk Meshmixer* (Autodesk, Inc., CA, USA). (Fig. 2c). After smoothing and removing bumps, indentations, and sharp edges, we imported the model into

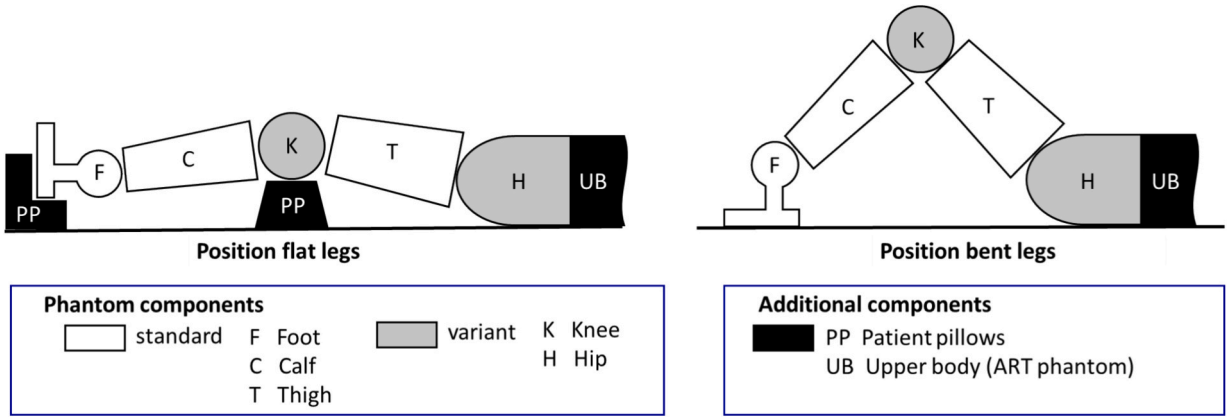

Fig. 1. Side view of the concept for the left side of the leg phantom, showing the phantom components and positions.

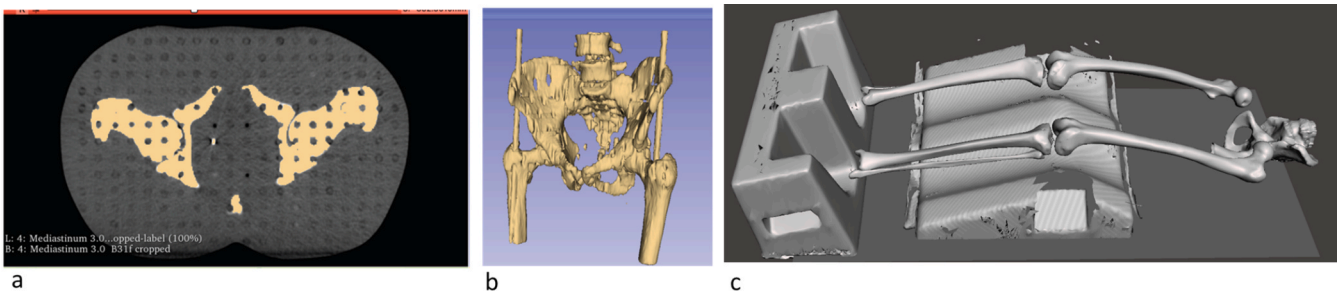

Fig. 2. From CT images to a 3D phantom model: a) transversal CT image of the ART phantom at the hip level with segmented bone structure. b) derived 3D pelvic bone model. c) STL models of patient pillows and bones, visualized in Meshmixer.

Autodesk Inventor (Autodesk, Inc., CA, USA), where we then designed each component of the leg.

Fig. 3 shows the 3D model of the complete leg phantom on the patient cushions and in the bent position. The leg phantom has a total length of 93.5 cm and a maximum width of 32.7 cm. For a more efficient manufacturing, we divided the outer shell of each component into multiple parts, based on size and assembly sequence. The bones were embedded within the outer shell, which is characterized by a thin wall

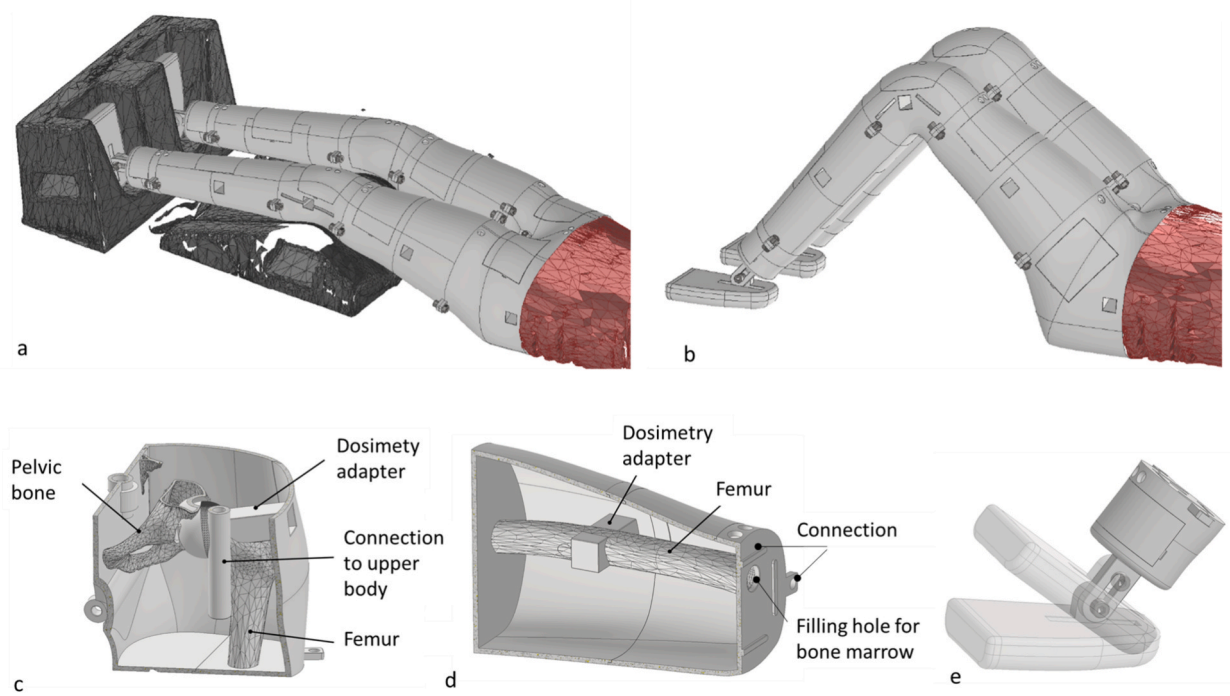

Fig. 3. CAD images of the leg phantom. a) flat position with patient pillows in black. b) bent position. c) view into the left hip. d) view into the left thigh. e) Foot with joint to realise different positions.

thickness to allow for filling with bone marrow surrogate after manufacturing (Fig. 3c). Since the outer shell itself will be filled with a soft tissue surrogate, each part is provided with filling holes or openings. Moreover, we designed plug-in and screw connections to assemble the individual components. A rod enables one to connect the hip to the upper body, fixing the slices of the ART phantom in place.

Four access points for an ionization chamber adapter are distributed along each leg: in the hip, calf, knee, and thigh, respectively. The chamber measuring points are always located in the centre of the bone (Fig. 3d). Additionally, two slots for radiochromic film are incorporated into the knee. To adjust the foot angle, we constructed a rail within the foot component. This ensures forward and backward movement by up to 2.5 cm and a rotation of up to 90° (Fig. 3e). The locking mechanism consists of a screw, so that the foot module can be used in both flat and bent leg phantom positions. All components were initially designed for the left leg and then mirrored to create the right leg. However, we had to slightly modify the hip components in order to optimize the connection to the ART upper body phantom, as the ART is not completely symmetrical.

2.4. Phantom manufacturing

All components of the leg phantom are additively manufactured with an *HP Designjet 3D* (*HP Inc.*, CA, USA) using the Fused Deposition Modeling (FDM) process (Fig. 4a, b) and an acrylonitrile butadiene styrene (ABS) material. Once additive manufacturing was complete, we removed the support material, manually as well as with a chemical solution bath, using the *HP Designjet 3D Removal System*.

In the next step, we coated all bone structures with two to three layers of plaster bandages for simulating the cortical bone (Fig. 4c). To protect the plaster from moisture, we then applied clear varnish as the final coating. Components that had to be divided into several segments, due to the limited printing space of the 3D printer, are connected and fixed with an adhesive (3 M Scotch-Weld SF20).

The final operation for completing the phantom was the choice of tissue surrogates: for the bone marrow, we prepared a mixture containing 75 % in weight of Vaseline and 25 % in weight of di-potassium hydrogen phosphate (K_2HPO_4). This mixture can be heated in a water bath and poured into the bones (Fig. 4d) [24,25]. Constant stirring and a temperature of at least 60 °C is needed to generate a homogeneous mixture. After having filled the bones and sealed them with a plug, we prepared the soft tissue mixture, consisting of i) a liquid mixture of agarose (2 wt%), ii) carrageenan (1.5 wt%), iii) $CaCO_3$ (2 wt%), and iv) water (94.5 wt%) [25,26]. Also in this case, we heated the mixture in a water bath to approximately 70 °C prior to filling up the hollow parts.

2.5. Phantom use in TBI

As described above, the total prescribed dose in TBI typically ranges between 2 and 12 Gy, with 2 Gy per fraction. Irradiations are usually performed twice a day with breaks of 8 to 12 h. In the myeloablative case, it is recommended to limit the mean dose to the lung to a maximum of 10 Gy [27,28]. We tested the phantom use in TBI for future comparison of two different techniques, namely, the static-field technique currently used in our institution and a so-called sweeping beam technique [9,10]. In both cases, we irradiated the whole-body phantom (ART phantom and leg phantom) with high-energy x-rays at a TrueBeam® medical linear accelerator (Varian Medical Systems, Palo Alto, USA), as specified below.

2.5.1. Whole-body CT images of phantom

To obtain whole-body CT images of the phantom, we used a so-called stitching scheme: (i) we imaged the phantom twice (head first and feet first, respectively) with our clinical CT scanner (SOMATOM Go.Open Pro, Siemens Healthineers, Munich, Germany). Since the maximum scan length is 130 cm, the two images overlap in the region of the lower torso. (ii) To obtain a common coordinate system between the two images, we placed three markers in the overlap region, at the phantom surface. (iii) We stitched the images by first using a landmark-based registration, implemented with the SimpleITK software package [29]. In order to further stabilize the registration performance, we then set the landmark registration as the initial point for an intensity-based rigid registration. In fact, the intensity-based registration takes not only the landmark position into account, but also the CT values within the whole region of overlap, thus resulting in a more accurate whole-body image. We then imported the whole-body CT images into the treatment planning system Eclipse™, version 16.1 (Varian Medical Systems, Palo Alto, USA) for treatment planning.

2.5.2. Static-field technique

The static-field technique implemented in our department consists of a combination of fixed-gantry, opposing-field arrangements. For a total dose of 12 Gy, five fractions are delivered with two opposing right-left lateral fields. The patient is positioned, supine and with bent legs, at an extended SSD of approximately 350 cm (see Fig. 5a). We correct for dose inhomogeneities due to different body thicknesses with the help of a dose build-up spoiler and PMMA compensators. During the sixth fraction, we combine anterior-posterior (AP) and posterior-anterior (PA) opposing fields and reduce lung dose to a maximum of 10 Gy by creating a patient-specific lung transmission block. The patient lies supine (or prone) with flat legs at an extended SSD of about 190 cm, at a short distance from the floor. The dose is delivered with three pairs of opposing AP-PA fields, having the isocenter in the head-neck, torso-

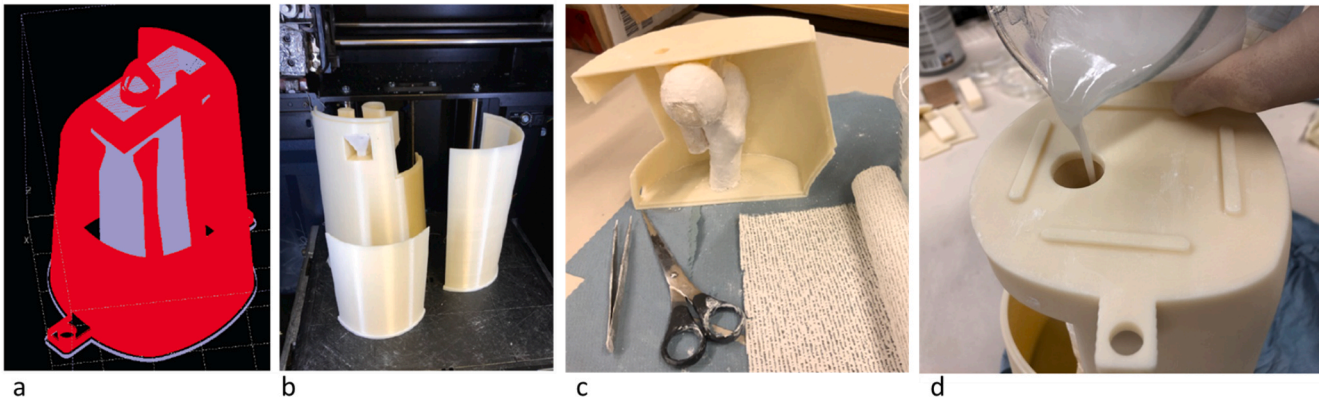

Fig. 4. Manufacturing process: a) Printing preparation, as visualized with the HP Designjet 3D Software Solution. b) FDM printing with the HP Designjet 3D printer. c) application of plaster to the bone structures. d) pouring the bone marrow mixture.

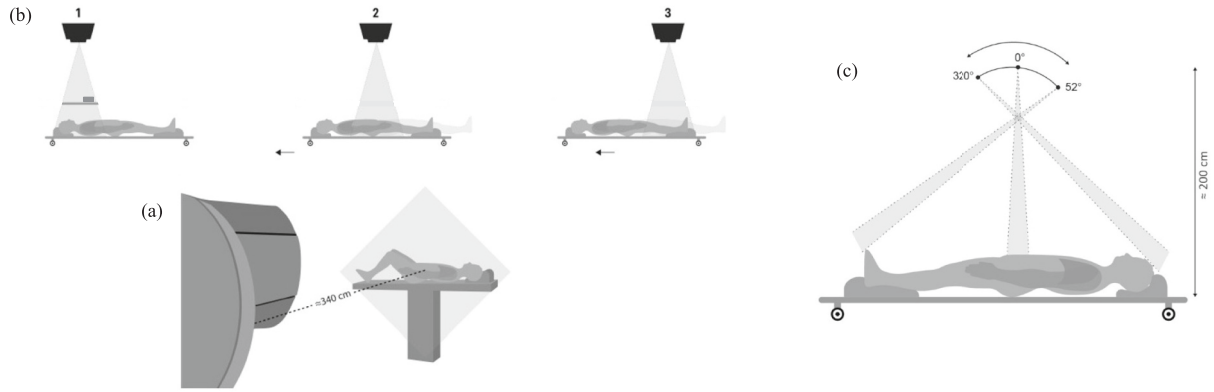

Fig. 5. Schematic representation of the TBI techniques to be compared. a) Static-field lateral irradiation. b) Static-field ventral irradiation with three isocenters and the use of lung blocks at the first isocenter. c) Sweeping-beam technique.

femur, and lower-extremity regions, respectively. The field sizes are determined based on body parameters, such as diameters and lengths (see Fig. 5b). The three isocenters are placed in such a way, that the fields are as close together as possible while minimizing overlap at the field junctions. Placed on a couch that can be translated, the patient is set to the first field position (head-neck). The field boundary on the patient's skin is then labelled to use as a guide for positioning of the subsequent treatment fields. The patient is then set to the third field position (legs), and after labelling the field boundary, the field size parameters for the second field (torso-upper legs) are also recorded. Lung transmission blocks are created based on patient anatomy and CT images, and placed in the beam during the AP-PA irradiation of the torso (Fig. 5b). Since the treatment planning system (TPS) in our institute is not commissioned for SSD >120 cm [30], we calculate the dose manually with the help of tabulated data [31]. The reference point for delivering the prescribed dose of 2 Gy is set to be the beam isocenter. For the static-field technique, we typically work with a 6 MV x-ray spectrum in the case of AP-PA irradiations and with 15 MV in the case of lateral irradiations, respectively.

2.5.3. Intensity-modulated sweeping-beam technique

For future modernization of the irradiation technique, which could avoid the production of lung blocks and allow for the use of standard treatment rooms, we are investigating an intensity-modulated sweeping-beam technique, similar to those introduced by Jahnke et al. [9] and Pierce et al. [10], which consists of two partial plans. The patient is positioned like for the static-field AP-PA irradiation (Fig. 5b) but, in this case, the gantry sweeps over the patient starting at an angle of approximately 50° and ending at about 320° (Fig. 5c). This approach requires CT-based radiation treatment planning, which we carried out with the Eclipse™ TPS, version 16.1 (Varian Medical Systems, Palo Alto, USA). We first needed to define some structures for plan optimization, in particular, body and lungs. Moreover, to ensure gantry rotation beyond head and feet, we extended the transversal CT images by one slice before the first and after the last layer, respectively. Each plan (AP and PA) includes two fields, 10 cm × 22 cm in size, rotating clockwise and counter-clockwise in the angular range 320°–52°, with collimator angles set at 5° and 355°, respectively. The sweeping-beam technique will be implemented with a 6 MV X-ray spectrum. The clinical use of this technique in our department will be established as soon as the TPS commissioning for extended SSDs will be completed, therefore the data shown is this work are limited to feasibility.

2.5.4. Dose measurements

We carried out first dose measurements to analyse the usability of the whole-body phantom. For the static-field TBI technique, we measured the absolute dose with an ionization chamber and dosimetry films, while we compared relative dose profiles for the SB technique. In particular, we positioned Gafchromic™ EBT3 dosimetry films (Ashland, Wilmington, USA) inside the phantom in the transversal plane in correspondence of relevant anatomical regions, such as head, thorax, abdomen, heap, and knee (see also Table 4 and Fig. 8). Moreover, we positioned a calibrated ionization chamber (CC04, IBA Dosimetry GmbH, Schwarzenbruck, Germany), embedded in a water-equivalent adapter, in correspondence of hips and knee, respectively. While the ionization chamber was calibrated in a secondary-standard laboratory in terms of dose to water, we calibrated the films at the TrueBeam® by placing them at the depth of maximum dose in a water-equivalent plate phantom and taking the ionization chamber as the reference.

3. Results

The results are structured into three key sections: CT imaging, dose verification of the static-field TBI technique, and dose-profile measurement to investigate the feasibility of the sweeping-beam technique. These aspects allow for a comprehensive evaluation of the phantom's performance and its potential applications in TBI.

3.1. CT imaging

Fig. 6 shows the complete whole-body phantom, both with flat (Fig. 6a) and bent legs (Fig. 6c) together with the newly designed and manufactured leg phantom. We replaced the lower part of the ART phantom (starting from slice no. 31) by the pelvic module developed in this study. The corresponding CT images show an excellent qualitative contrast between soft tissue and bone surrogates. We measured the CT numbers in rectangular regions of interest, 30 mm × 50 mm in size, and calculated mean values from several slices. The average results are summarized in Table 2, together with literature data for comparison. A long-time analysis, carried out by scanning the leg phantoms four times over a period of 14 months, demonstrates that, while the bone-marrow surrogate remains stable in terms of volume, the soft-tissue surrogate tends to dry up, as can also be seen in Fig. 6b. Also, the materials become more compact with time: the mean CT numbers for soft tissue increase during the first few months, while those for bone marrow decrease, with their standard deviations continuously decreasing. For both mixtures, the CT numbers remained then stable one year after manufacturing (Table 3).

3.2. Dose verification of the static-field TBI technique

Table 4 summarizes the mean dose values obtained with the dosimetry films. Here, we evaluated an area of (2.5 × 2.5) cm^2 in the central part of each film, i.e., approximately along the phantom midline.

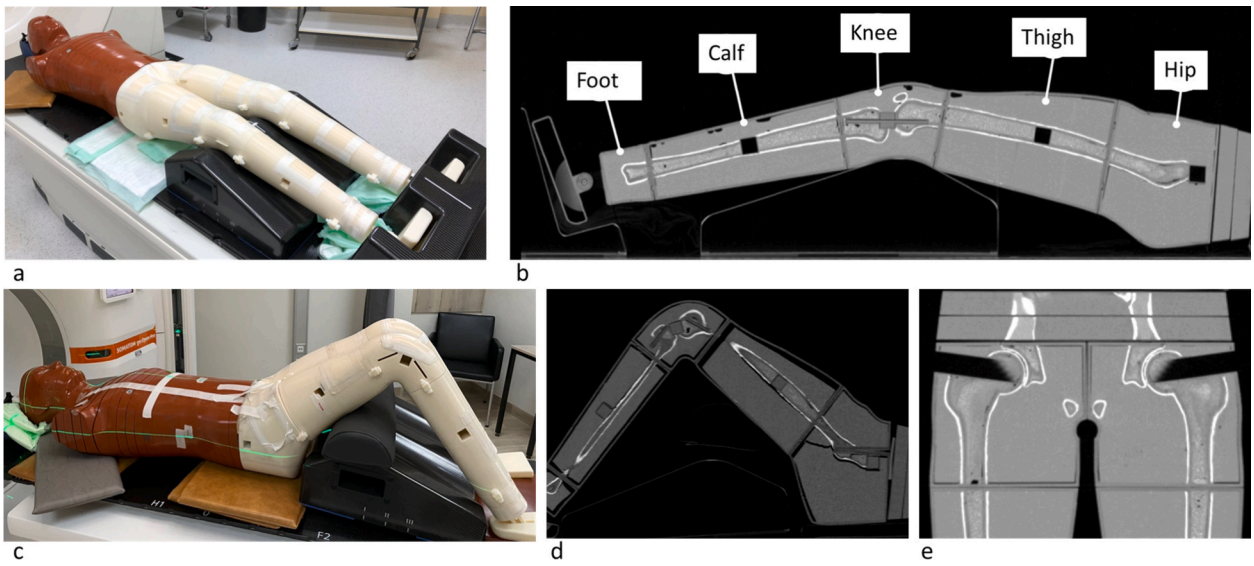

Fig. 6. Final whole-body phantom, consisting of ART torso and the leg phantom prototype manufactured in this work. a) Legs in flat position. b) Example of sagittal CT image of legs in flat position, scanned a few days after production. The black squares correspond to the positions of water-equivalent adapters (or plugs) to insert an ionization chamber for dose measurements. c) Legs in bent position. d) Example of sagittal CT image in bent position, with inserted plugs, scanned 14 months after production, showing that the soft-tissue surrogate lost some volume and that air fills gaps between surrogate and external material. e) Coronal CT image of the pelvic region, showing a smooth connection between ART torso and leg phantom.

Table 2
CT numbers in terms of Hounsfield Units (HU) measured during this work for relevant tissue surrogate types and corresponding values found in the literature. The values for the leg phantoms are those measured one day after manufacturing.

Tissue	Literature values	ART phantom	Leg phantom
Soft tissue	20–90 HU [32] 50 HU [33] 50–60 HU [34]	−1.5 ± 20 HU	35 ± 15 HU
Bone marrow	100–250 HU [35] −120–600 HU [24]	210 ± 50 HU	160 ± 90 HU
Compact bone	250–1200 HU [35] Up to 2000 HU [33]	990 ± 230 HU	750 ± 200 HU

Table 3
CT numbers in terms of Hounsfield Units (HU) measured during this work for the soft-tissue and bone-marrow mixtures at different time points after manufacturing.

Time after manufacturing in days	1	5	60	430
Soft tissue	35 ± 15 HU	35 ± 8 HU	50 ± 5 HU	50 ± 5 HU
Bone marrow	160 ± 90 HU	160 ± 40 HU	90 ± 8 HU	100 ± 10 HU

We also measured the absorbed dose with the ionization chamber, placed in the appropriate insert, at two different points (hip and knee). If considering the relative experimental uncertainty of about ±15 % (confidence interval of 95 %) for film dosimetry, these preliminary results are in good agreement with the prescribed dose.

3.3. Feasibility study of the sweeping beam technique

Thanks to the whole-body CT-images obtained with the procedure described in Section 2.5.1, we tested the feasibility of the SB technique and methods for accurate patient positioning (Fig. 7). Despite the fact that the treatment planning system does not calculate the dose correctly, Fig. 8 demonstrates that the horizontal and vertical profiles of the

Table 4
Dose measurements in correspondence of some relevant anatomic areas, for the static-field AP-PA irradiation. The prescribed dose was 2 Gy. The films were placed between two slices of the ART phantom (with slice numbers in brackets) or in the knee insert. The ionization chamber was placed in the appropriate insert (see Fig. 6). The total experimental uncertainty was determined according to the ISO Guide to the expression of uncertainty in measurement (GUM) with a coverage factor k = 2 [36].

Position	D_{film} in Gy	D_{IC} in Gy
Head (0–1)	1.85 ± 0.28	
Head (3–4)	2.23 ± 0.33	
Upper thorax (11–12)	2.39 ± 0.36	
Thorax (16–17), soft tissue	2.18 ± 0.33	
Thorax (16–17), lung tissue	0.44 ± 0.07	
Abdomen (21–22)	2.15 ± 0.32	
Field overlap Hip (30–31)	2.30 ± 0.34	
Hip		2.05 ± 0.04
Knee	2.30 ± 0.34	2.11 ± 0.04

calculated and measured dose in several phantom sections are in good agreement when normalized to the dose value at the profile center. This good relative agreement proves that, despite the fact that the commissioning our treatment planning system is still missing for extended SSD, the dose optimization algorithm works in a reliable way. Moreover, these profiles and the 3D dose representation in Fig. 9 demonstrate that the dose distribution is homogeneous within ±10 %. Finally, the lung dose can be reduced by about 20–30 %, while the static-field technique, combined with lung blocks, enables a lung dose reduction of 80 %. As a consequence, for a myeloablative treatment, the sweeping beam technique should be used for all six fractions in order to ensure that the mean dose to the lungs does not exceed 10 Gy.

4. Discussion and conclusion

The increasing number of studies that have been carried out in the last 10–15 years to introduce conformal TBI techniques confirms the necessity for detailed commissioning and for a high level of dosimetric accuracy, especially for the design of future clinical trials in this field [12]. In particular, dosimetry audits on TBI are still missing and future

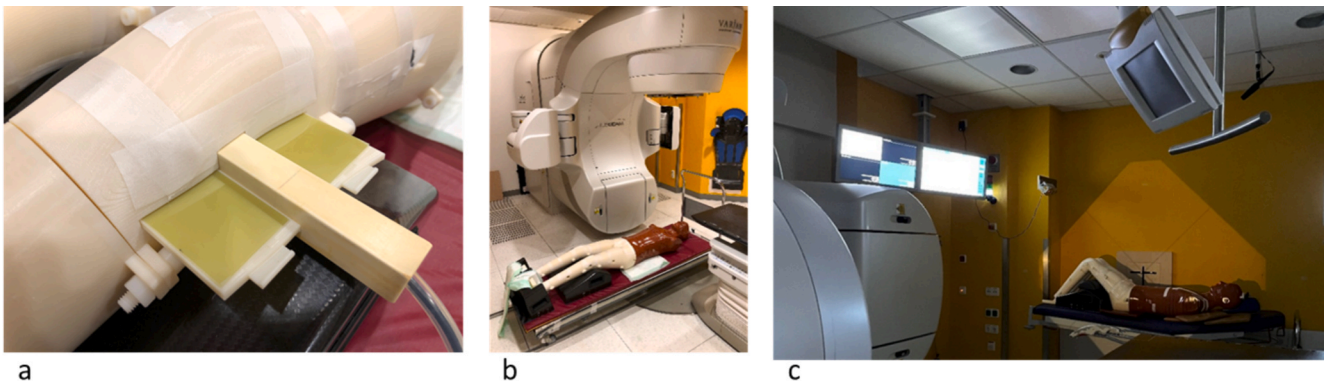

Fig. 7. Example of phantom positioning for dose measurements at extended SSDs. a) Dosimeter placement inside corresponding compartments in the knee module, encompassing ionization chamber and radiochromic film. b,c) Set-up at the linear accelerator for ventral and lateral irradiation, respectively.

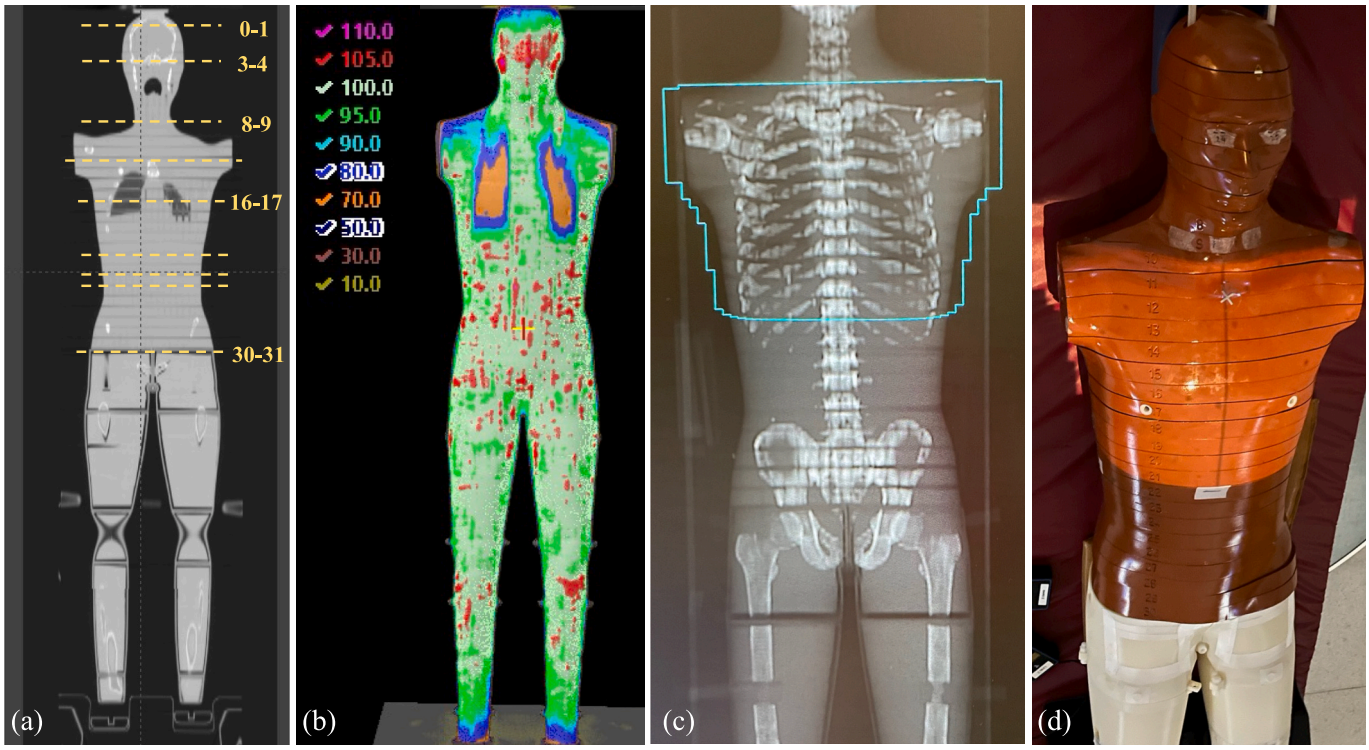

Fig. 8. (a) Whole-body CT image for treatment planning. The dashed lines show the position of dosimetry films and the corresponding slice numbers as orientation. (b) Planned 3D dose distribution for the SB technique. (c,d) Phantom positioning for accurate SB irradiation. The creation of a set-up field with the MLC (a) allows for accurate alignment on the treatment couch thanks to the light-field visualisation (d). Significant anatomical features (e.g., clavicles and ribs) provide guidance to this purpose.

work in this direction will also have benefits for further irradiation treatments involving the whole body, such as total-marrow irradiation (TMI) and total-nodal irradiation (TNI) [12]. This work contributes to the advancement of quality assurance in TBI by developing a cost-effective anthropomorphic phantom of the lower extremities, which can be used in combination with a commercially-available torso phantom to obtain a phantom of the whole body.

The leg phantom design is modular, thus allowing for the simulation of different leg positions. Moreover, thanks to the integration of flexible inserts, it is possible to measure dose in relevant positions. Here, we show results for measurements with ionization chambers as well as radiochromic films, as an example. Such flexibility enables one to compare different TBI approaches and a complex commissioning of the used treatment planning system. The cost effectiveness of the leg phantom is guaranteed by an additive manufacturing approach, consisting in the 3D printing of hollow leg, bone, and pelvis structures and the use of agarose- and Vaseline-based mixtures to mimic the x-ray attenuation properties of soft tissue and bone marrow, respectively. Furthermore, the use of gypsum allowed us to mimic cortical bone.

We investigated the suitability of the leg phantom by simulating TBI with the static-field technique that is well established in our institute. First dose measurements, carried out with dosimetry films, an ionization chamber, and OSL dosimeters, are in agreement, within ± 10 %, with the prescribed dose of 2 Gy, which is promising for further studies. Moreover, we were able to demonstrate that the whole-body phantom, obtained by combining the developed leg phantom and the ART torso, is suitable for several levels of quality assurance in TBI. In fact, we could explore an “image-stitching” method to obtain CT images of the whole body, which we also used for dose optimization of an intensity-modulated SB technique. During this feasibility study, we also

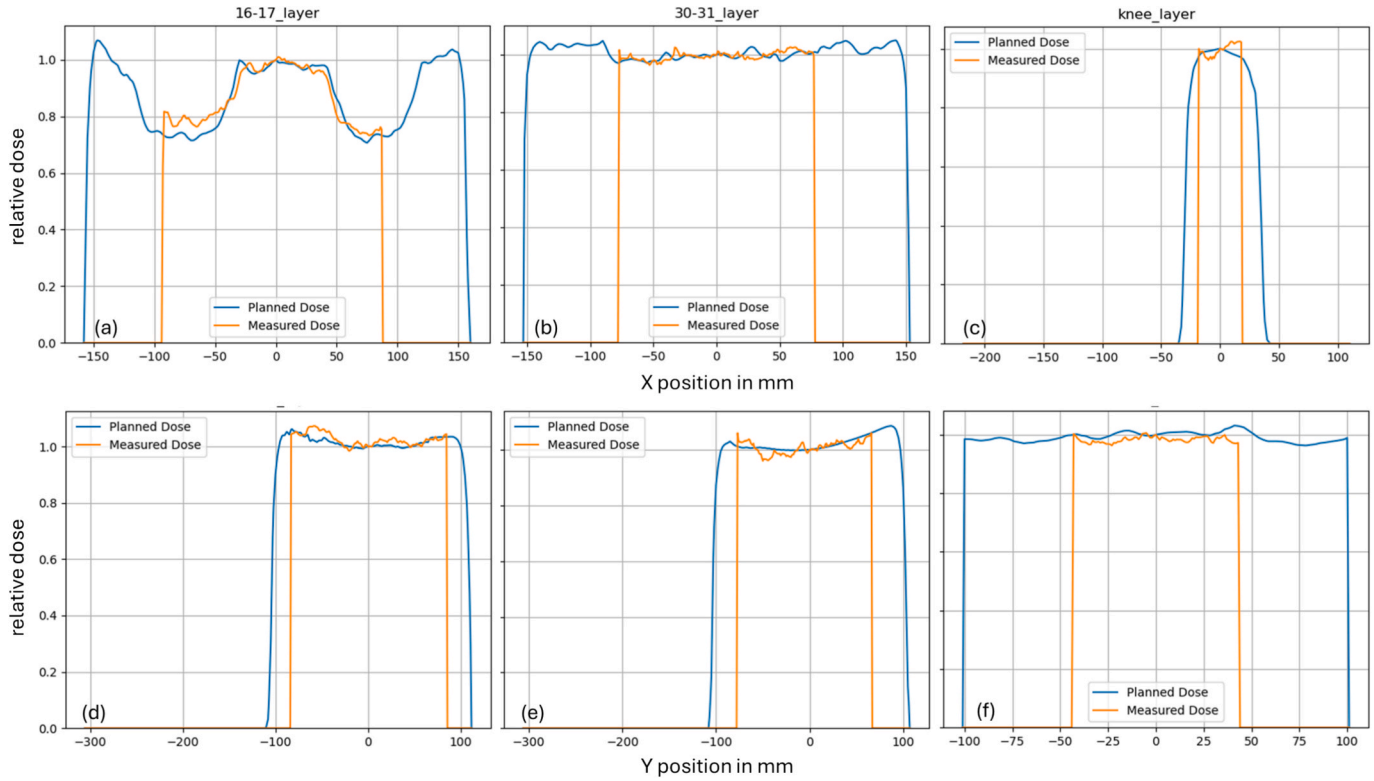

Fig. 9. Relative dose profiles, in X direction (a–c) and in Y direction (d–f), in three phantom regions: lungs (a,d), pelvis at the interface between ART torso and leg phantom (b,e), and knee (c,f). The X-position is horizontal (left–right), the Y-position is vertical (top–bottom) along the phantom central line, respectively. The dose profiles are normalized to each other at (0,0).

introduced a simple approach for patient alignment at an extended SSD of approximately 190 cm. This is based on the use of set-up fields and will be extended and applied for image verification in the future. A precise alignment of the whole body is not critical in TBI, since all radiation-sensitive organs to be spared lie in the torso. For this reason, several groups investigating conformal TBI opted for simplifications. For example, in some cases, CT imaging was performed only up to the middle thigh and then an extended CT was created by replicating a slice from the middle thigh, as often as necessary to obtain the full patient length [10,11]. However, for plan optimization in TMI or TNI, the use of phantom legs with realistic anatomy could improve dose accuracy. In addition, realistic legs for radiation treatment planning and verification would improve the quality assurance in TBI for isocentric techniques, such as VMAT and Tomotherapy. In this case, two separate treatment plans are optimized for the head-first and the feet-first CT scans, respectively. The two plans need then to be optimized to obtained the correct dose distribution in the overlapping region, which is usually around the pelvis or the upper thigh [12,13]. Therefore, to verify the dose in this overlapping region, additional dosimetry films might be inserted between (i) the torso and the hip, (ii) the hip and the thigh, and (iii) between the thigh and the calf, respectively.

This study has some limitations, which we will discuss in the following. First, after production, the properties of the soft-tissue surrogate changed during the first weeks, mostly due to water loss. In fact, the HU-values of the surrogates increased by more than 40 % for soft tissue, and decreased by about 60 % for bone marrow, respectively. However, after this significant change, the CT numbers remained stable for at least one year and the x-ray contrast remained appropriate. Furthermore, the CT numbers became more homogenous, with potentially less heterogeneity in the calculated dose. We intend to improve the sealing of the phantom modules to reduce the formation of air gaps in the future. Moreover, further investigations will be necessary to establish the dose uncertainty related to variations in the material water content. The second limitation for the use in TBI studies is the incomplete commissioning of our treatment planning system for extended SSDs, so that the dose verification for the sweeping-beam techniques is limited, up to now, to the relative comparison between the calculated and the measured dose. We will complete the dosimetry study for expended SSDs and investigate isocentric techniques in the future.

In conclusion, we can state that the modular leg phantom developed in this work will facilitate further TBI analysis and, with slight modifications, it can be extended for quality assurance in TMI and TNI. While we do not plan to commercialize the phantom, we have provided a detailed description of its development and manufacturing to support reproducibility. Departments interested in implementing the phantom for their own research are welcome to contact the corresponding author for further discussion.

Declaration of competing interest

The authors declare that they have no known competing financial interests or personal relationships that could have appeared to influence the work reported in this paper.

Acknowledgements

Publishing fees are supported by the Hamburg University of Technology (TUHH). The authors would like to thank Jannik Theiding (TUHH), Maria Jäckel, Volker Platz, and Ilse König (UKE) for their valuable support during this project.

References

[1] Gruen A, Ebell W, Wlodarczyk W, Neumann O, Kuehl JS, Stromberger C, et al. Total Body Irradiation (TBI) using Helical Tomotherapy in children and young adults undergoing stem cell transplantation. Radiat Oncol 2013;8:92. https://doi.org/10.1186/1748-717X-8-92.

[2] Juric MK, Ghimire S, Ogonek J, Weissinger EM, Holler E, van Rood JJ, et al. Milestones of hematopoietic stem cell transplantation – from first human studies to current developments. Front Immunol 2016;7:470. https://doi.org/10.3389/fimmu.2016.00470.
[3] Hansen AT, Rose HK, Yates ES, Hansen J, Petersen JBB. Two compound techniques for total body irradiation. Tech Innov Patient Support Radiat Oncol 2022;21:1–7. https://doi.org/10.1016/j.tipsro.2021.11.006.
[4] Hoeben BAW, Pazos M, Seravalli E, Bosman ME, Losert C, Albert MH, et al. ESTRO ACROP and SIOPE recommendations for myeloablative Total Body Irradiation in children. Radiother Oncol 2022;173:119–33. https://doi.org/10.1016/j.radonc.2022.05.027.
[5] Hoeben BAW, Wong JYC, Fog LS, Losert C, Filippi AR, Bentzen SM, et al. Total body irradiation in haematopoietic stem cell transplantation for paediatric acute lymphoblastic leukaemia: review of the literature and future directions. Front Pediatr 2021;9:774348. https://doi.org/10.3389/fped.2021.774348.
[6] Quast U. Total body irradiation—review of treatment techniquesin Europe. Radiother Oncol 1987;9(2):91–106. https://doi.org/10.1016/s0167-8140(87)80197-4.
[7] Kirby N, Held M, Morin O, Fogh S, Pouliot J. Inverse-planned modulated-arc total-body irradiation. Med Phys 2012;39(5):2761–4. https://doi.org/10.1118/1.4705366.
[8] Fog LS, Hansen VN, Kjær-Kristoffersen F, Berlon TE, Petersen PM, Mandeville H, et al. A step and shoot intensity modulated technique for total body irradiation. Tech Innov Patient Support Radiat Oncol 2019;10:1–7. https://doi.org/10.1016/j.tipsro.2019.05.002.
[9] Jahnke A, Jahnke L, Molina-Duran F, Ehmann M, Kantz S, Steil V, et al. Arc therapy for total body irradiation–a robust novel treatment technique for standard treatment rooms. Radiother Oncol 2014;110(3):553–7. https://doi.org/10.1016/j.radonc.2013.12.009.
[10] Pierce G, Balogh A, Frederick R, Gordon D, Yarschenko A, Hudson A. Extended SSD VMAT treatment for total body irradiation. J Appl Clin Med Phys 2019;20(1):200–11. https://doi.org/10.1002/acm2.12519.
[11] Frederick R, van Dyke L, Hudson A, Pierce G. Advanced automated treatment planning for total body irradiation: Implementation and effects on standardization. Phys Med 2023;112:102623. https://doi.org/10.1016/j.ejmp.2023.102623.
[12] Misson-Yates S, Cunningham R, Gonzalez R, Diez P, Clark CH. Optimised conformal total body irradiation: a heterogeneous practice, so where next? Br J Radiol 2023;96(1144). https://doi.org/10.1259/bjr.20220650.
[13] Seravalli E, Bosman ME, Han C, Losert C, Pazos M, Engström PE, et al. Technical recommendations for implementation of volumetric modulated arc therapy and helical tomotherapy total body irradiation. Radiother Oncol 2024;197:110366. https://doi.org/10.1016/j.radonc.2024.110366.
[14] Izewska J, Lechner W, Wesolowska P. Global availability of dosimetry audits in radiotherapy: the IAEA dosimetry audit networks database. Phys Imaging Radiat Oncol 2018;5:1–4. https://doi.org/10.1016/j.phro.2017.12.002.
[15] Erler-Zimmer GmbH &Co. KG. [December 12, 2024]; Available from: https://erler-zimmer.de.
[16] Kyoto Kagaku Co., Ltd. [December 12, 2024]; Available from: https://www.kyotokagaku.com/en/.
[17] Radiology Support Devices Inc. [December 12, 2024]; Available from: https://rsdphantoms.com/.
[18] Wegner M, Krause D. 3D printed phantoms for medical imaging: recent developments and challenges. J Mech Sci Technol 2024;38(9):4537–43. https://doi.org/10.1007/s12206-024-2407-8.
[19] Verein Deutscher Ingenieure. VDI 2221: Design of technical products and systems Model of product design. VDI-Richtlinien 2019.
[20] Wegner M, Schmiech J, Sobirey E, Krause D, Gargioni E. Requirement analysis in medical phantom development: a survey tool approach with an illustrative example of a multimodal deformable pelvic phantom. Front Phys 2024;12. https://doi.org/10.3389/fphy.2024.1416601.
[21] Krause D, Gebhardt N. Methodische Entwicklung modularer Produktfamilien: Hohe Produktvielfalt beherrschbar entwickeln. Berlin: Springer Verlag; 2018.
[22] Krause D, Gebhardt N. Methodical Development of Modular Product families: developing High Product Diversity in a Manageable Way. Berlin: Springer Verlag; 2023.
[23] Fedorov A, Beichel R, Kalpathy-Cramer J, Finet J, Fillion-Robin J-C, Pujol S, et al. 3D Slicer as an image computing platform for the Quantitative Imaging Network. Magn Reson Imaging 2012;30(9):1323–41. https://doi.org/10.1016/j.mri.2012.05.001.
[24] Niebuhr NI, Johnen W, Güldaglar T, Runz A, Echner G, Mann P, et al. Technical note: Radiological properties of tissue surrogates used in a multimodality deformable pelvic phantom for MR-guided radiotherapy. Med Phys 2016;43(2):908–16. https://doi.org/10.1118/1.4939874.
[25] Breslin T, Paino J, Wegner M, Engels E, Fiedler S, Forrester H, et al. A novel anthropomorphic phantom composed of tissue-equivalent materials for use in experimental radiotherapy: design, dosimetry and biological pilot study. Biomimetics (Basel) 2023;8(2). https://doi.org/10.3390/biomimetics8020230.
[26] Singhrao K, Fu J, Wu HH, Hu P, Kishan AU, Chin RK, et al. A novel anthropomorphic multimodality phantom for MRI-based radiotherapy quality assurance testing. Med Phys 2020;47(4):1443–51. https://doi.org/10.1002/mp.14027.
[27] Sampath S, Schultheiss TE, Wong J. Dose response and factors related to interstitial pneumonitis after bone marrow transplant. Int J Radiat Oncol Biol Phys 2005;63(3):876–84. https://doi.org/10.1016/j.ijrobp.2005.02.032.
[28] Lohr F, Wenz F, Schraube P, Flentje M, Haas R, Zierhut D, et al. Lethal pulmonary toxicity after autologous bone marrow transplantation/peripheral blood stem cell transplantation for hematological malignancies. Radiother Oncol 1998;48(1):45–51. https://doi.org/10.1016/s0167-8140(98)00045-0.
[29] Lowekamp BC, Chen DT, Ibáñez L, Blezek D. The design of SimpleITK. Front Neuroinform 2013;7:45. https://doi.org/10.3389/fninf.2013.00045.
[30] Varian Medical Systems. Eclipse photon and electron algorithms reference guide. Palo Alto, CA; 2017.
[31] Dutreix A, Bjarngard B, Bridier A, Mijnheer B, Shaw J, Svensson H. Monitor unit calculation for high energy photon beams: ESTRO Booklet 3. Leuven, Belgium: Garant Publishers; 1997.
[32] D'Souza W, Madsen EL, Unal O, Vigen KK, Frank GR, Thomadsen BR. Tissue mimicking materials for a multi-imaging modality prostate phantom. Med Phys 2001;28(4):688–700. https://doi.org/10.1118/1.1354998.
[33] Alkadhi H, Leschka S, Stolzmann P, Scheffel H. Wie funktioniert CT?: Eine Einführung in Physik, Funktionsweise und klinische Anwendungen der Computertomographie. Berlin, Heidelberg: Springer-Verlag GmbH Berlin Heidelberg; 2011.
[34] Engelke K, Museyko O, Wang L, Laredo J-D. Quantitative analysis of skeletal muscle by computed tomography imaging-State of the art. J Orthop Translat 2018;15:91–103. https://doi.org/10.1016/j.jot.2018.10.004.
[35] Kalra A, Developing FE. Human Models from medical images. In: Basic Finite Element Method as Applied to Injury Biomechanics. Elsevier; 2018. p. 389–415.
[36] Joint Committee for Guides in Metrology. Guide to the expression of uncertainty in measurement: Technical Report BIPM:100, International Organization for Standardization; 2004.